Hydroprocessed Esters and Fatty Acids (HEFA) model for Large Eddy Simulation

Thomas Lesaffre
lesaffre@cerfacs.fr
Bénédicte Cuenot and Eleonore Riber

Centre Européen de Recherche et de Formation Avancée en Calcul Scientifique (CERFACS)
Energy and Propulsion
Toulouse
France

Said Taileb and Jean-Baptiste May-Carle

Safran Tech
Paris-Saclay
France

ABSTRACT

The use of Sustainable Aviation Fuels (SAFs) impacts the operability limits of aviation gas turbines. The difference in behavior compared to conventional jet fuel is either attributed to the fuel physical or chemical properties. Therefore, new faithful fuel models are required to recover the fuel behavior in numerical simulations. In this work, fuel models reproducing a SAF obtained with the Hydroprocessed Esters and Fatty Acids (HEFA) conversion process are derived to be used in Large Eddy Simulation. They rely on a multi-component surrogate and an Analytically Reduced Chemistry (ARC) mechanism to be sensitive to variations in fuel physical and chemical properties. Two surrogates with different volatilities are combined with two ARC mechanisms containing either only high-temperature or both low- and high-temperature chemistry pathways. To investigate the difference in behavior, the 4 possible combinations for the fuel model are compared in the simulation of a swirl-stabilized spray academic burner, showing features relevant to current aviation engine combustors. For stable operating conditions, the flames obtained for the 4 cases have a comparable behavior showing marginal differences that can be attributed to the variations in volatility or reactivity. More differences can be observed at a leaner equivalence ratio near blow-out as the cases with only high-temperature chemistry pathways fail to sustain a flame while the operating condition is experimentally stable. This was attributed to a too low heat release rate in the stabilization zone where, without sufficient compensation, heat losses ultimately induced a decrease in temperature detrimental for the flame stabilization.

.

INTRODUCTION

The aviation sector is required to lower its greenhouse gas emissions towards the 2050 horizon[1]. One approach to reach this goal is to substitute conventional jet fuels with alternative fuels[2]. Significant efforts have been made to certify conversion pathways for Sustainable Aviation Fuel (SAF) production that can replace partially jet fuels in today's engine architecture. As of July 2023, 11 conversion processes have been approved while 11 other conversion processes are still under evaluation*. Hydroprocessed esters and fatty acids (HEFA) conversion process is one of the most mature pathways and leads to an important reduction in carbon emissions[2,3]. The certification of SAF through the ASTM D4054 remains expensive as it involves important fuel volume for direct testing[4]. Three figures of merit are particularly tested during the fuel approval process as they were identified critical for safety: lean blow-out (LBO), altitude relight, and cold start. LBO was shown experimentally to be sensitive to physical properties (such as volatility) and chemical properties (such as autoignition propensity) depending on the configuration and the operating conditions[5,6,7]. Therefore, a need of faithful fuel models arises for numerical simulations as high-fidelity simulations may reduce the cost of SAF certification process by helping select the fuel candidate with adequate properties.

Most early numerical works regarding aviation fuels relied on a simple fuel modeling strategy consisting of a mono-component surrogate and a globally-fitted kinetic scheme, such as a 4-step mechanism for a pseudo-species C12H23[8,9] or a 2-step mechanism for a pseudo-species C10H20[10,11]. However, the simplicity of these models limits their application when investigating the behavior of SAFs in combustion chambers, as mono-component surrogates are similar for SAFs and conventional jet fuels. Therefore, more complex fuel models were introduced to take into account the fuel sensitivity in simulations. First, more representative surrogates for Jet A and SAFs were developed[12,13,14]. Multi-component surrogates can reproduce preferential vaporization effects that affect the flame structure[15,16]. These more complex surrogates then call for more complex chemical kinetics. Detailed kinetic mechanisms[17] have existed for a long time in the literature but the number of species they contain together with their stiff characteristic chemical times have prevented their use in simulations. Reduction techniques to obtain smaller but representative mechanisms have been therefore developed and permitted the study of fuel behavior with real chemistry effects in Large Eddy Simulations (LES)[12,18].

The efforts towards more representative fuel modeling have led to new investigations showing fuel effects on the stable flame structure. In the context of the American National Jet Fuel Combustion Program (NJFCP)[4], Pignatelli et al.[19] showed that marginal differences between two alternative jet fuels appear in the combustion behavior. Akerblom et al.[20] linked differences in spray penetration depths with fuel volatility. Soriano et al.[21] identified differences in flame stabilization dynamics with faster local re-ignition for Jet A compared to a SAF (Alcohol-to-Jet sample). A similar effort was performed in Europe with the H2020 JET Fuel SCREENing and Optimization (JETSCREEN) project[22]. Eckel et al.[23] studied the conventional jet fuel spray flame structure with a multi-component vaporization model and reduced chemistry modeling, showing the benefits of finite rate chemistry inclusion in LES. Multi-component surrogates and reduced chemistry were also used to investigate differences in flame structure, showing differences in combustion regime due to differences in

* https://www.icao.int/environmental-protection/GFAAF/Pages/Conversion-processes.aspx

volatility[15,24].

More complex fuel effects exist, on the pollutant formation or burner operability, that realistic fuel models are able to describe. The PAH growth chemistry pathways, relevant for soot formation, were included in reduced mechanisms to study the behavior of conventional jet fuel[26,27] and alternative jet fuels[27]. From the operability perspective, the fuel impact on the LBO limit of an academic combustor relevant to aeronautical burner was largely investigated during the NJFCP[28,29,30], showing a quantifiable difference in the predicted LBO limit that can be either attributed to differences in fuel volatility or reactivity.

Following the preceding works reported in the literature, a fuel model able to accurately capture both physical and chemical properties of real fuels is proposed in this work for a HEFA fuel, combining a multi-component surrogate and an Analytically Reduced Chemistry (ARC) mechanism[31]. The fuel model is then used to simulate the lean flame stabilization and near blow-out behavior in an academic burner using Large Eddy Simulation.

The paper is organized as follows. First, the methodology followed for the derivation of the fuel model for HEFA is presented. Then, the results obtained with the HEFA fuel model in the LES of an academic burner are presented and analyzed.

1.0 FUEL MODEL

Both fuel composition and fuel oxidation kinetics must be modeled to describe the fuel behavior in a combustion chamber. The development of the HEFA fuel surrogate is discussed in Section 1.1. Section 1.2 presents the chemical mechanism developed for the HEFA surrogate.

1.1 HEFA surrogate

1.1.1 Choice of properties

Surrogates are mixtures containing few components (typically from 1 to 6) that mimic the real fuel properties. They have been extensively used for conventional jet fuels[33,34,35]. If the validity of fuel surrogates for jet fuels has been debated in the literature[36,37], the simpler composition of SAFs makes the surrogate approach more relevant and significantly lowers the potential uncertainties of the surrogate representativity of the real fuel. In this work, a surrogate composition optimization tool has been derived, inspired by the work of Narayanaswami et al.[35] and Kim et al.[34]. The choice of the target properties to be reproduced by the surrogate has been largely discussed in the literature. Dooley et al.[33] proposed a methodology to emulate the real fuel chemical behavior by targeting four properties: molecular weight (MW), hydrogen-to-carbon ratio (H/C), threshold sooting index (TSI) and derived cetane number (DCN). Kim et al.[34] also considered the liquid density, the liquid viscosity, the surface tension, and the distillation curve. MW and H/C of the mixture can be computed analytically from the composition and molecule formula. This is not the case for TSI and DCN, which usually rely on a simple mole average rule. However, such correlations have a limited interest for numerical simulations since they do not reflect the surrogate behavior in the simulation. Indeed, the ignition propensity and soot precursors production in simulations are driven by the chemical kinetics mechanism used. Therefore, depending on the choice of the chemical kinetics mechanism, the ignition propensity of a species can differ importantly. Therefore, these two properties are not considered in this work for the surrogate choice.

From the previous discussion, the HEFA surrogate is here established based on four properties: MW, H/C, the lower heating value, and the distillation curve. The first three properties help reproduce the chemical behavior of the real fuel whereas its volatility is captured by targeting the distillation curve. The liquid viscosity and surface tension are not considered in this work as they are not directly accounted for in the LES approach. The accuracy of the surrogate liquid density is checked a posteriori, by comparison with the real fuel properties. Mole average is used as mixture rule to compute fuel blend properties, with the lower heating value estimated from the formation enthalpy of the species. The distillation curve is computed following a simple batch distillation model described in [34], which is similar to [37].

The real fuel properties are estimated from a two-dimensional gas chromatography (GCxGC) and an ASTM D86 distillation curve measurement, obtained for a HEFA fuel sample from the JETSCREEN campaign. The gas chromatography of the fuel is presented in Fig. 1. GCxGC allows the identification of the fuel composition by chemical families, but does not allow to identify individual isomers as their individual signals overlap [38]. This means that isomers are lumped together in the chromatography, usually by the number of carbon elements they contain. This is an intrinsic limitation of the method as the degree of isomerization can substantially affect the combustion properties, particularly autoignition [39]. This could be quite important as the fuel is mainly composed of i-alkanes (82.32%). Two other families are identified in the fuel: n-alkanes (15.27%) and cyclo-alkanes (2.17%) whereas only traces of aromatics are found (0.24%).

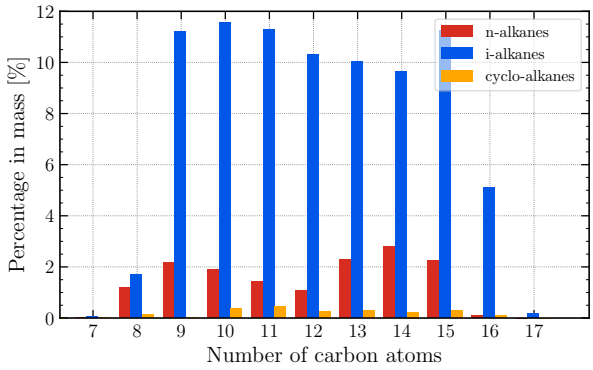

Figure 1: Gas chromatography of the HEFA sample fuel considered in this study

1.1.2 Surrogates

To accurately describe the chemical families in the real fuel, 4 species are selected to build the surrogate: i-C8H18, i-C12H26, i-C16H34 and n-C12H26, i.e., i-alkanes and n-alkanes only. The composition is determined through an optimization procedure, minimizing an objective function built from the 4 selected properties. In order to investigate the whole range of compositions and ensure the determination of a "global" optimum, different initial guesses are automatically generated. The composition of the obtained surrogate (Surrogate 1, S1) is given in Table 1. A second surrogate (Surrogate 2, S2) is derived by relaxing the constraint on the distillation curve, i.e., decreasing its weight in the objective function. Indeed, a close

match with the experimental distillation curve leads to an important amount of i-C16H34 in Surrogate 1, which may not be representative of the real fuel volatility. This may be attributed to the fact that ASTM D86 standard is not exactly representative of the true vapor-liquid equilibrium used for the numerical estimation of the distillation curve. Corrections have been proposed in the literature but they cannot be generalized[34].

Table 1: Surrogate mole fractions [%]

	i-C8H18	**i-C12H26**	**i-C16H34**	**n-C12H26**
Surrogate 1 (S1)	15.4	38.6	30.6	15.4
Surrogate 2 (S2)	15.4	58.6	10.6	15.4

The main properties of the real fuel and both surrogates are reported in Table 2. The properties targeted in the optimization procedure show a really good agreement with the real properties, with relative errors close to 1%. It is also interesting to notice that even if the liquid density was not targeted in the optimization, the values obtained for both surrogates is very close to the value measured for the real fuel. Finally, the proportion of the chemical families in the surrogates is faithful to the composition of the real fuel even if slightly higher due to the absence of cyclo-alkanes.

Table 2: Comparison between the surrogates and real fuel main properties

	REAL FUEL	**S1**	**S2**
LHV [MJ/kg]	44.18	44.29	44.41
H/C	2.167	2.159	2.170
MW [g/mol]	171.1	178.3	167.1
n-alkanes [mass%]	15.27	14.7	15.7
i-alkanes [mass%]	82.32	85.3	84.3
l [kg/m3] at 15°C	752	760.8	749.7

Figure 2 displays the comparison of the distillation curves between the measurement for the real fuel and the numerical estimation for the surrogates. S1 has a slightly higher distillation temperature at the beginning of the distillation whereas S2 has a better agreement with the experimental points when less than 10% of the volume has evaporated. Conversely S1 is closer to the experimental points after the vaporization of 40% of the volume while S2 appears to be too volatile in this zone. The greater error for S2 is due to the relaxation of the constraint on the distillation curve in the optimization procedure.

1.2 ARC mechanisms

Reactive simulations require a chemical mechanism to describe the combustion process. The use of detailed chemical mechanisms remains too computationally challenging to be directly included in LES solvers, in terms of cost and stiffness. The ARC methodology[31] has been proposed to overcome this issue, reducing detailed chemical mechanisms to make them affordable for LES, while keeping the main chemical pathways to accurately describe the combustion process[18]. In this work, ARCANE[40] is used to perform the mechanism reduction with an automated and efficient algorithm. ARCANE relies on different methods: Direct Relation Graph with Error Propagation for species and reaction reduction[41], chemical lump-

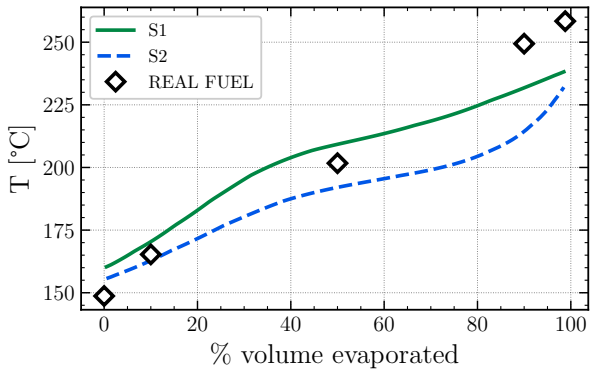

Figure 2: Comparison of the experimental and numerical distillation curves

ing[42], and stiffness removal through the Quasi Steady State Approximation[31]. The detailed mechanisms chosen for this work are the CRECK mechanism C1-C16 with high-temperature chemical pathways (CRECK_2003_TOT_HT) and the CRECK mechanism C1-C16 with high and low-temperature chemical pathways (CRECK_2003_TOT_HT_LT)[17]. The objective is to derive reduced mechanisms with and without low-temperature chemistry pathways to assess their effect on the behavior near LBO in LES, as it was shown to be important in the literature[43].

Two types of cases are targeted during the reduction: 1D premixed flames and 0D isochoric reactors. The operating conditions targeted during the reduction process are summarized in Table 3. The 1D premixed flame conditions targeted are close to each other for the high-temperacture only (HT) case as well as the high- and low-temperature (HT_LT) case, only the inlet temperature differs by 50 K. For the 0D isochoric reactors, different conditions are targeted. Lower temperatures are targeted in the HT_LT case at a lean equivalence ratio, more relevant for LBO applications.

Table 3: Operating conditions targeted during the reduction process

	T [K]	**P [Pa]**	ϕ
1D_HT	400	1e5	0.6-1-1.4
1D_HT_LT	350	1e5	0.6-1-1.4
0D_HT	1200-1300-1400-1500	1e5	1.0
0D_HT_LT	800-1000-1200-1400	1e5	0.8

The reduction process is based solely on cases with S1 composition. Behavior for S2 is validated a posteriori. Maximum relative error thresholds are prescribed during the reduction process, summarized in Table 4. Note the higher error threshold prescribed for the autoignition delay time of the HT_LT case, to obtain a significantly reduced mechanism.

The resulting mechanisms obtained after reduction contain 30 transported species, 374 irreversible reactions and 20 species in a quasi-steady state for HT conditions (called ARC_HT in the following) and 32 transported species, 385 irreversible reactions and 26 species in a quasi-steady state for HT_LT conditions (called ARC_HT_LT). The ARC mechanisms have been validated against the detailed mechanisms for an extended range of operating conditions.

Table 4: Relative maximum error threshold [%] for the reduction

	1D_sl	**1D_Tmax**	**0D_tig**
HT	5	1	15
HT_LT	5	1	20

The ARC laminar flame speed displayed in Fig. 3 shows a really good agreement with the detailed mechanism for S1 (left) and S2 (right). Maximum relative error compared to the detailed mechanism occurs for equivalence ratios between 0.9 and 1.1 where the laminar flame speed is important. It is interesting to notice that even if the reduction did not contain cases for S2, the errors compared to the detailed mechanism are remarkably low, even lower than for S1. Figure 4 shows the autoignition delay times for $\phi = 0.6$ (top) and $\phi = 1.0$ (bottom). All the detailed and ARC mechanisms provide similar results above 1000 K. Autoignition delay times are slightly smaller for the ARC mechanisms from 1100K to 1400K whereas the detailed mechanisms have smaller autoignition delay times above 1400 K. However, the differences between the mechanisms are marginal. Important differences exist for temperatures lower than 1000K, particularly for the ARC_HT as no case below 1000K ignition delay time was targeted during the reduction. The ARC_HT_LT reproduces with good fidelity the autoignition delay time for S1 up to 800 K, below that temperature the ARC_HT_LT becomes more reactive compared to the detailed mechanism with low-temperature pathways as it was not targeted in the reduction. The errors become noticeable for S2 for a higher temperature, approximately 850 K. But overall, the agreement is quite good considering that the reduction was performed for an equivalence ratio of 0.8 for the ARC_HT_LT.

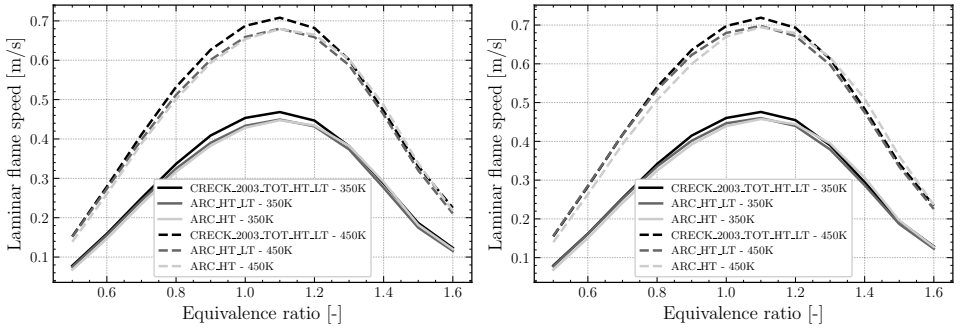

Figure 3: Laminar flame speeds of S1 (left) and S2 (right) at 1 bar and 2 initial temperatures 350K and 450K, as a function of the equivalence ratio for the detailed reference mechanism and the 2 ARC mechanisms

2.0 APPLICATION TO A SPRAY-FLAME BURNER

The fuel model presented in Section 1 is used to investigate the fuel effect on lean flame stabilization. The model is tested in the academic Spray-Stabilized Burner (SSB)[44,45] operated at DLR.

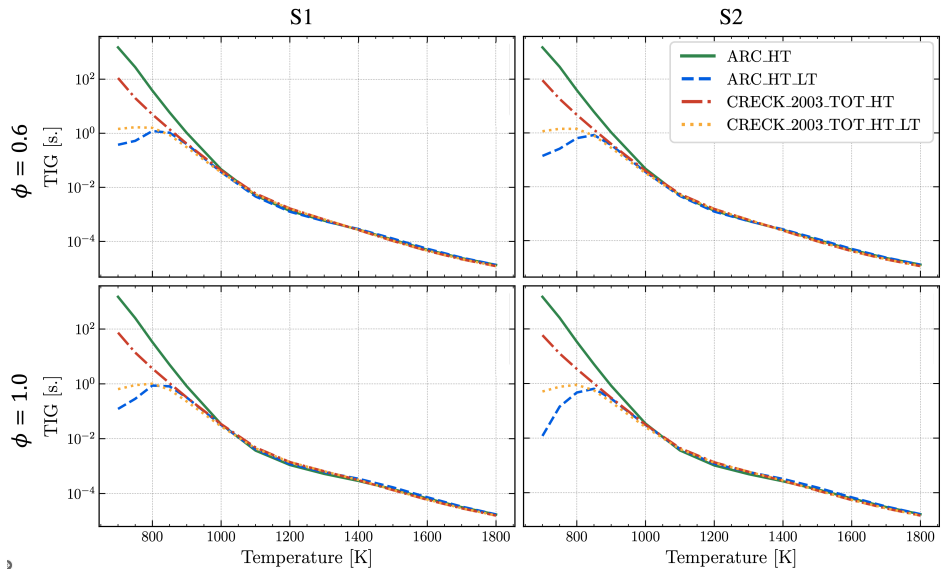

Figure 4: Autoignition delay times of S1 (left) and S2 (right) at 1 bar and at an equivalence ratio of 0.6 (top) and 1.0 (bottom), as a function of the temperature for the 2 detailed reference mechanisms and the 2 ARC mechanisms

2.1 Experimental setup

The SSB configuration is an academic swirl-stabilized combustion chamber equipped with a prefilming airblast atomizer and a double-stage swirler (Fig. 5a). This technology is similar to the one used in typical aeronautical combustion chambers, which makes the SSB a good test bench even if it is operated at atmospheric pressure. The combustion chamber has a cross-section of 85 x 85 mm for a height of 169mm (Fig. 5b). Lateral walls are made of quartz to provide optical access to the flame.

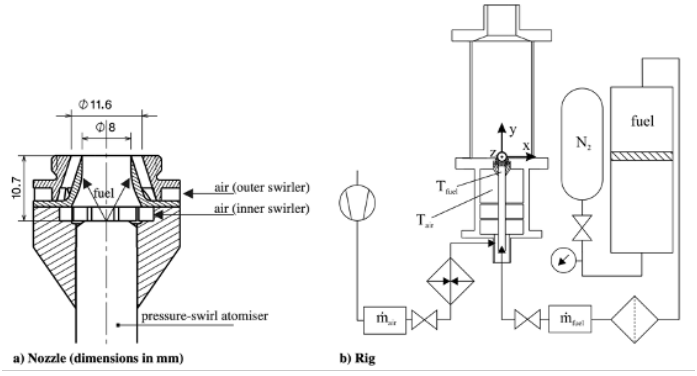

Figure 5: SSB experimental setup (from[44])

An aviation fuel screening campaign has been carried out in the SSB to study the fuel impact on stabilized flames and on the LBO limit during the JETSCREEN campaign[22]. The stable operating conditions are summarized in Table 5.

Table 5: Stable Operating Conditions

w_{air} [g/s]	w_{fuel} **[g/s]**	T_{air} **[K]**	**P [atm]**	T_{fuel} **[K]**
4.3	2.361e-4	323.15	1	303.15

The experimental methodology to capture LBO consists of several steps, described in[46] and illustrated in Fig. 6. From the stable operating conditions, the flame is first stabilized near LBO (first at $\phi = 0.6$, then 80 g/h above the expected LBO limit). The time spent at this operating condition point has not been measured. From this operating point, the fuel mass flow rate is reduced at a constant rate of 0.5 g/h/s until the flame blows out.

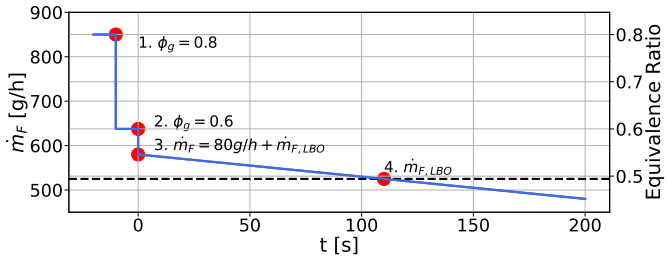

Figure 6: Sketch of the experimental procedure for LBO detection (from[24])

2.2 Numerical setup

The computational domain corresponding to the experimental setup contains 2.33 million nodes and 13.2 million tetrahedral elements. The swirler vanes are discretized with at least 8 points through their section. The cell sizes in the flame stabilization region are of the order of the laminar flame thickness. This mesh resolution for an LES could be considered coarse. However, investigating the LBO behavior remains expensive as it requires long physical simulated times, as suggested by Fig. 7 where the fluid residence time in the combustion chamber is quite large, particularly in the Inner Recirculation Zone (IRZ) and Outer Recirculation Zone (ORZ). Therefore, the mesh resolution is a tradeoff between the accuracy and the cost of the simulation. The choice of mesh resolution is validated against the cold flow velocity profiles in Appendix A.

The simulations were performed with the in-house solver AVBP[47] to solve the 3D compressible reactive Navier-Stokes equations using the Large Eddy Simulation (LES) approach. Lax-Wendroff scheme[48], 2nd order both in time and space is used to discretize the convection terms. A second-order finite element scheme is used for diffusion terms. The explicit time integration relies on a single Runge-Kutta step. Subgrid flame-turbulence interactions are accounted by the TFLES model coupled with the Charlette constant efficiency model[49]. A dynamic formulation is used, based on a flame sensor relying on the O2 consumption

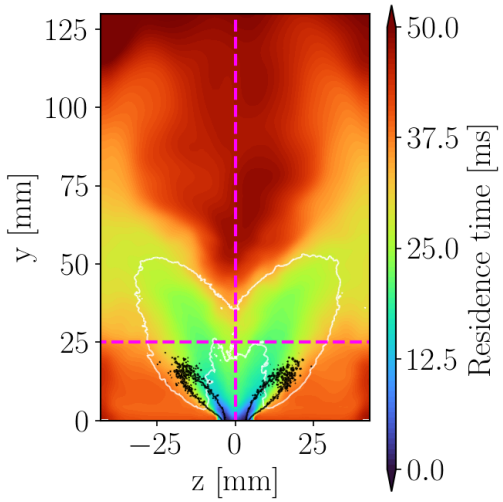

Figure 7: Transversal cut in the computational domain colored by the fluid residence time in the chamber (computed through a transport equation[54]). White and black isolines correspond to a heat release rate of 3e7 W/m^3 and a liquid loading of 0.01 respectively. Magenta dashed lines correspond to y = 25mm and x = z = 0 mm cuts.

source term[50]. The TFLES model is activated only in the premixed zone identified with a flame index[51]. The NSCBC approach[53] is used for the inlet and outlet boundary conditions. Experimental temperature profiles are imposed at the walls[24].

The droplets, considered as point particles, are tracked using a Lagrangian formalism. Assuming a dilute spray regime, the mass evolution of the droplets can be computed from the isolated droplet evaporation models. A multi-component extension of the Abramzon-Sirignano model[32] is used. The FIM-UR approach is used to mimic the fuel injection and atomization[52]. In this procedure, a numerical Rosin-Rammler droplet-size distribution is imposed (with d_{32} =37 μm and q=2.6) to match the experimental diameter profiles obtained for Jet-A[24], measured in the chamber for the stabilized operating conditions reported in Table 5. As no experimental data are available for the spray when reducing the fuel flow rate and changing the fuel, the parameters of the Rosin-Rammler function are kept the same in this study. The sensitivity to this choice is discussed in Appendix B.

Four cases are compared to investigate the effect of fuel volatility and low-temperature chemistry. The two surrogates are coupled with the two ARC mechanisms presented in Section 1. The four cases are labeled: S1_ARC_HT, S2_ARC_HT, S1_ARC_HT_LT and S2_ARC_HT_LT.

3.0 RESULTS

The results section is divided into two parts. First, the different fuel models are compared on the stable lean operating point reported in Table 5. Then, an experimentally stable point near LBO (ϕ=0.6) is studied.

3.1 Stable flame condition

The stable flame condition has been thoroughly investigated experimentally for Jet A with various diagnostics. However, there is a lack of data for HEFA. Therefore, a comparative study of the numerical results is proposed in this section, while Jet A experimental results are reported only for information. Simulation results are averaged for approximately 120ms for each case after convergence to a steady state.

The flame shape is similar for all the cases as indicated by the time-averaged heat release rate isolines in Fig. 8, exhibiting a typical M-shape. However, small differences can be observed as the cases with low-temperature chemistry pathways (ARC_HT_LT) shows a more intense heat release rate in the two branches of the M-flame. Moreover, the central part of the M-flame is larger for the more volatile surrogate (S2), particularly for the ARC_HT cases. These differences can also be observed through the integrated heat release rate profile along the chamber axis in Fig. 9. Both ARC_HT_LT cases display a higher peak of heat release rate near 40 mm along the axis, corresponding to the end of the intense zone. A small shift in the heat released can be observed when comparing S1 and S2 results but the differences are small.

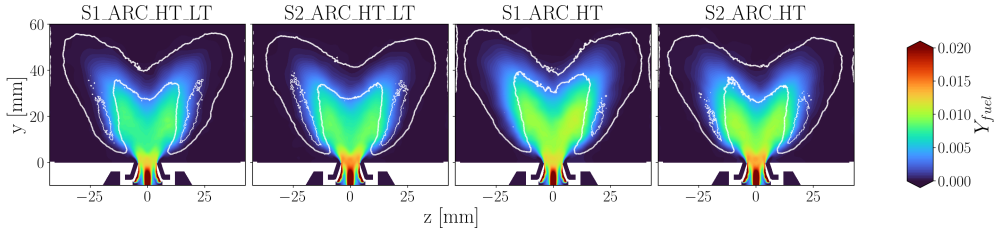

Figure 8: Time-averaged field of gaseous fuel mass fraction in the central cut plane. Thick and thin iso-lines correspond to a heat release rate of 3e7 and 1e8 W/m^3 respectively

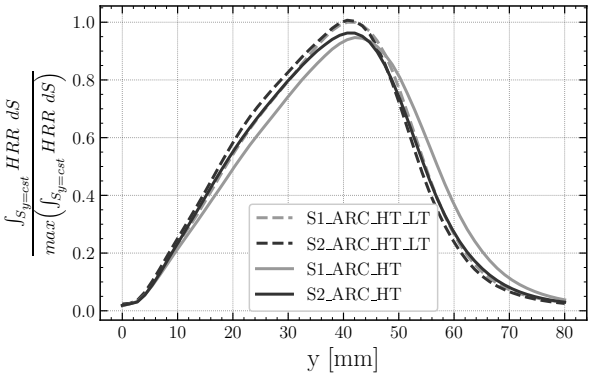

Figure 9: Time-averaged normalized heat release profile along the axis of the chamber

From the temperature perspective, all the cases exhibit similar results, displayed in Fig. 10. At y = 25mm, S2 cases show a slightly higher temperature in the center of the chamber while S1 cases show higher temperature closer to the chamber walls from 10 mm for

S1_ARC_HT_LT and from 30 mm for S1_ARC_HT. Along the chamber central axis (x = z = 0mm), the differences in temperature remain limited. The experimental data for Jet A provided for indication show a similar behavior to the numerical results, even if higher differences are observed. These discrepancies were also observed in previous work in the literature [23,24] and could not be clearly attributed to bias in the measurement or approximations from numerical models.

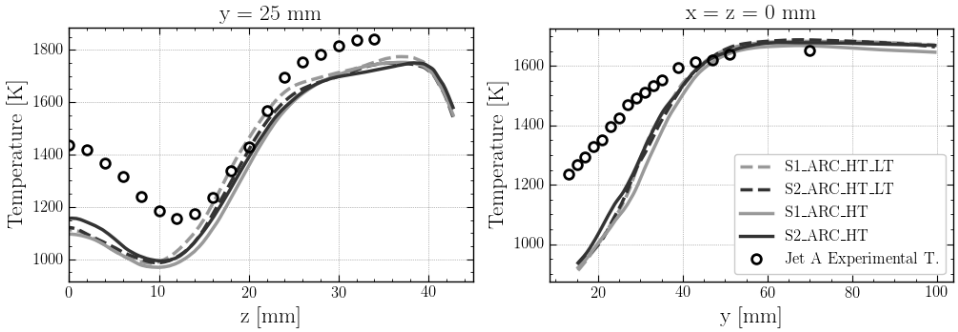

Figure 10: Time-averaged temperature profiles at y = 25mm (left) and x = z = 0mm (right)

Figure 8 also shows the field of gaseous fuel mass fraction with a higher proportion for the S2 cases near the swirler exit. The gaseous fuel mass fraction is the result of the production due to the vaporization of the liquid fuel and the chemical consumption. The profile of the integrated vaporization rate is displayed in Fig. 11. Two main peaks can be observed: the first peak is very close to the injection, corresponding to the vaporization before the creation of the liquid film in the swirler , while the second peak is located around 12 mm in the chamber, where the liquid spray sees an important increase in temperature as it starts interacting with the flame. The differences in vaporization appear to be limited in the chamber, as it was the case for the vaporization of isolated droplet at high temperature. A closer look at the vaporization profile in the swirler (Fig. 11 - right) indicates a significant difference in the vaporization rate where S2 cases exhibit a higher peak than S1 cases. The mass evaporated is also higher for S2 at the exit of the swirler up to 2.5 mm in the chamber.

The chemical consumption of the surrogate fuel species, controlled by the chemical kinetics scheme, is also dependent on the local amount of available fuel vapor, which is driven by the mixing and the vaporization of the liquid fuel. This is illustrated in Fig. 12 where differences can be attributed either to the fuel availability (highlighted by differences between S1 and S2 cases) or either to the rate of reaction (highlighted by the differences between the ARC_HT and ARC_HT_LT cases). S2 cases show a higher peak of fuel consumption around y = 15 mm in the chamber, that can be attributed to the higher fuel mass fraction visible near the swirler exit (Fig. 8) associated to the higher volatility of S2. The fuel consumption becomes higher for S1 after approximately 30 mm in the chamber. The fuel consumption is also higher for ARC_HT_LT than ARC_HT cases around 15 mm, while the shift in consumption occurs around 30 mm where the consumption becomes higher for ARC_HT.

The differences between the four cases are further highlighted by investigating the fuel chemical consumption by species, illustrated in Fig. 13. The higher consumption at 15 mm for the ARC_HT_LT cases is associated to a faster consumption of all the fuel species but the difference is particularly visible for i-C8H18 that shows a really fast consumption compared to

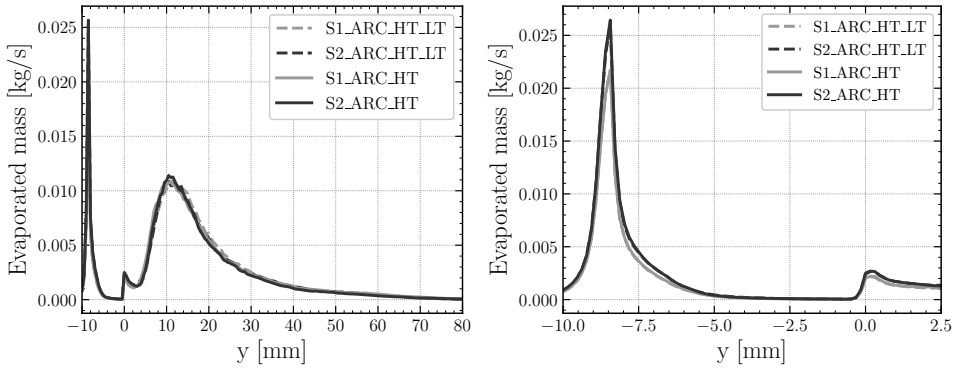

Figure 11: Time-averaged evaporated mass profile along the axis of the chamber up to 80 mm (left), zoomed from -10 to 5 mm (right)

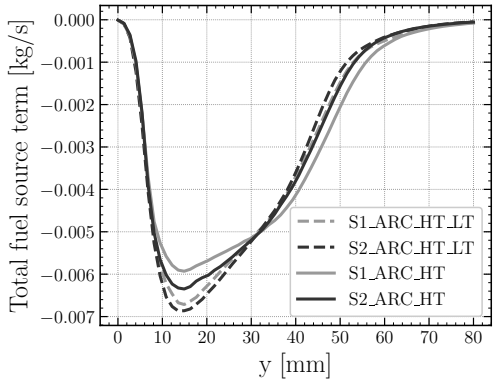

Figure 12: Time-averaged consumption profiles of all fuel species along the axis of the chamber

the ARC_HT cases, which exhibit a late consumption peak towards 35 mm. The fuel volatility difference is due to a different surrogate composition as seen by the i-C12H26 and i-C16H34 consumption profile. As i-C12H26 evaporates faster, it exhibits a consumption peak towards 12 mm, while the maximum consumption for i-C16H34 is reached around 16 mm. Moreover, i-C16H34 consumption happens further in the chamber compared to i-C12H26, which explain the differences in the total fuel consumption profile in Fig. 12.

The results on the stable operating conditions show that the different fuel models exhibit a similar behavior in the simulations, showing a similar flame shape even if small differences related to the fuel volatility or chemical reactivity are observed. This is expected as the difference in volatility is small and that the behavior for the stable point is mainly driven by the flame propagation properties, which is similar for all the chemical kinetics scheme as depicted in Fig. 3.

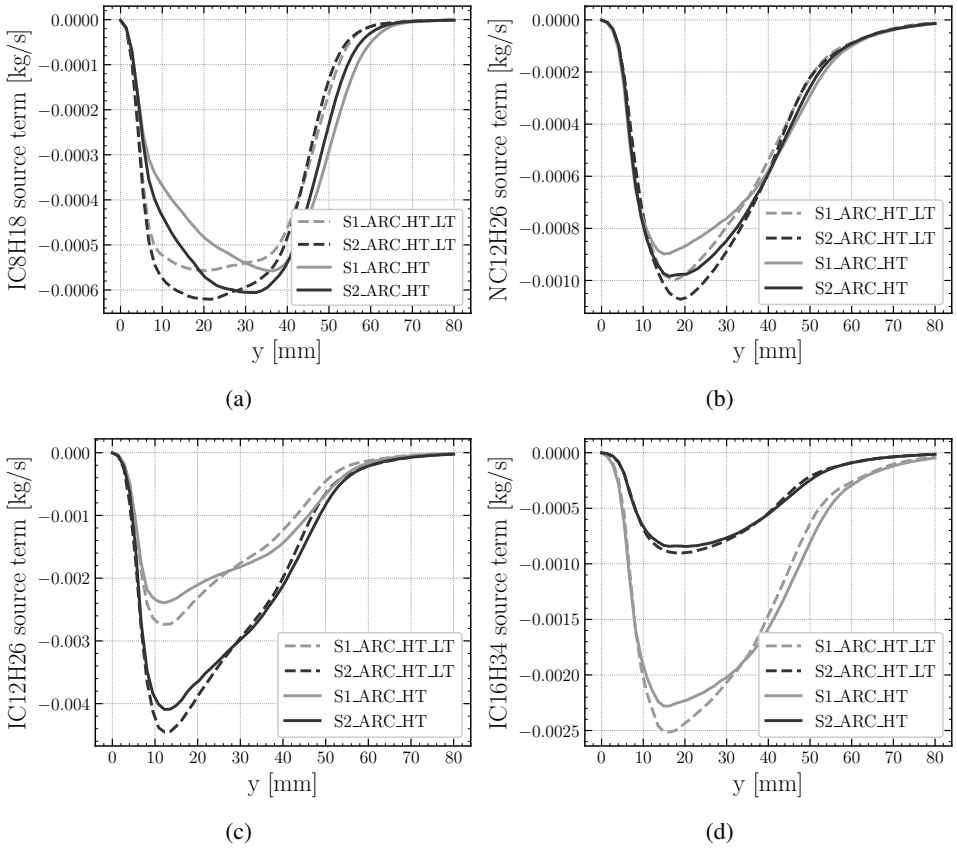

Figure 13: Time-averaged fuel consumption displayed by species along the axis of the chamber: (a) IC8H18, (b) NC12H26, (c) IC12H26 and (d) IC16H34

3.2 Near LBO behavior

Near blow-out behavior is expected to be more impacted by the variation of fuel properties as the behavior of the flame may not be entirely driven by propagation as the flame speed reduces importantly at very lean equivalence ratio. As in the experimental methodology, the equivalence ratio is reduced from ϕ = 0.8 to ϕ=0.6 in the simulations. The resulting time evolution of the thermal power is displayed in Fig. 14. It can be observed that contrary to experiment where the flame stays stable at ϕ=0.6, the 2 ARC_HT cases exhibit a flame fading up at 40ms to global extinction at 60-70ms. On the contrary, the 2 ARC_HT_LT cases show a stable behavior. These differences in behavior between the fuel chemistry models are further investigated in this section.

The evolution of the local equivalence ratio based on the chemical elements is displayed for the 4 cases in Fig. 15. It can be observed that the evolutions of the local equivalence ratio in the IRZ and in the ORZ are very slow. The local equivalence ratio in the ORZ remains higher than 0.6 for approximately 45 ms while the IRZ has still an equivalence ratio of approximately 0.7 after 60 ms. These slow evolutions are the result of the longer flow residence times in these

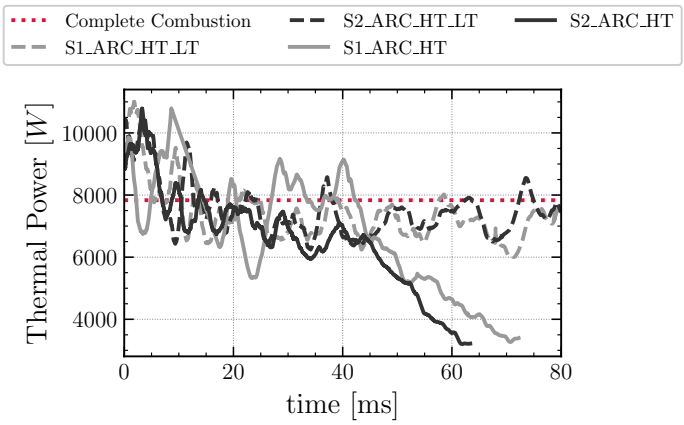

Figure 14: Evolution of the thermal power going from the stable point at ϕ=0.8 to the experimentally stable point near LBO (ϕ=0.6)

zones, shown in Fig. 7: the residence time is approximately 40 ms in the ORZ and around 50 ms in the IRZ. Interestingly, the flames for the ARC_HT start to fade once the equivalence ratio is significantly reduced in the ORZ.

The temperature evolutions, presented in Fig. 16 for the 4 cases, are also marked by the long residence times in the chamber. The IRZ remains at high temperature for all the cases. In the ORZ however, differences appear: if both ARC_HT_LT cases sustain a high temperature, both ARC_HT cases exhibit a continuous decreasing through time. This is further highlighted by the time evolution of the mean temperature in the ORZ for the 4 cases in Fig. 17. The ORZ is identified with the following criteria: a zone of burnt gases ($Y_{O2} < 0.13$) with negligible heat release rate (HRR < 1e7 W/m^3) and located below y = 40 mm as indicated by the fluid residence time in Fig. 7. As the temperature in the ORZ is the balance between the heat provided the flame, the mixing with fresh gases before the flame foot and the wall heat losses, the two branches of the M-flame in the ARC_HT cases do not burn sufficiently to provide enough heat to balance the heat losses. On the other hand, a steady temperature seems to be reached for the ARC_HT_LT cases after 60 ms for S1 and 70 ms for S2. This can be attributed to a more intense heat release rate of the flame branches stabilized in the shear layer with the ORZ, as it was the case for the stable operating condition (see Fig. 8). Therefore, the balance between the flame and the heat losses for the ARC_HT_LT cases is sufficient to sustain a high temperature in the ORZ which in turn help the flame stabilization.

CONCLUSION

In this work, fuel models for a Sustainable Aviation Fuel (SAF), called HEFA, have been derived to investigate the sensitivity to fuel properties in Large Eddy Simulation (LES). Particularly, the behavior near Lean Blow-Out (LBO) is investigated as it was shown experimentally to be impacted by variations in fuel physical and chemical properties. To do so, both fuel composition and fuel oxidation kinetics have been modeled, allowing to describe the real fuel behavior in a combustion chamber. Multi-component surrogates and Analytically Reduced

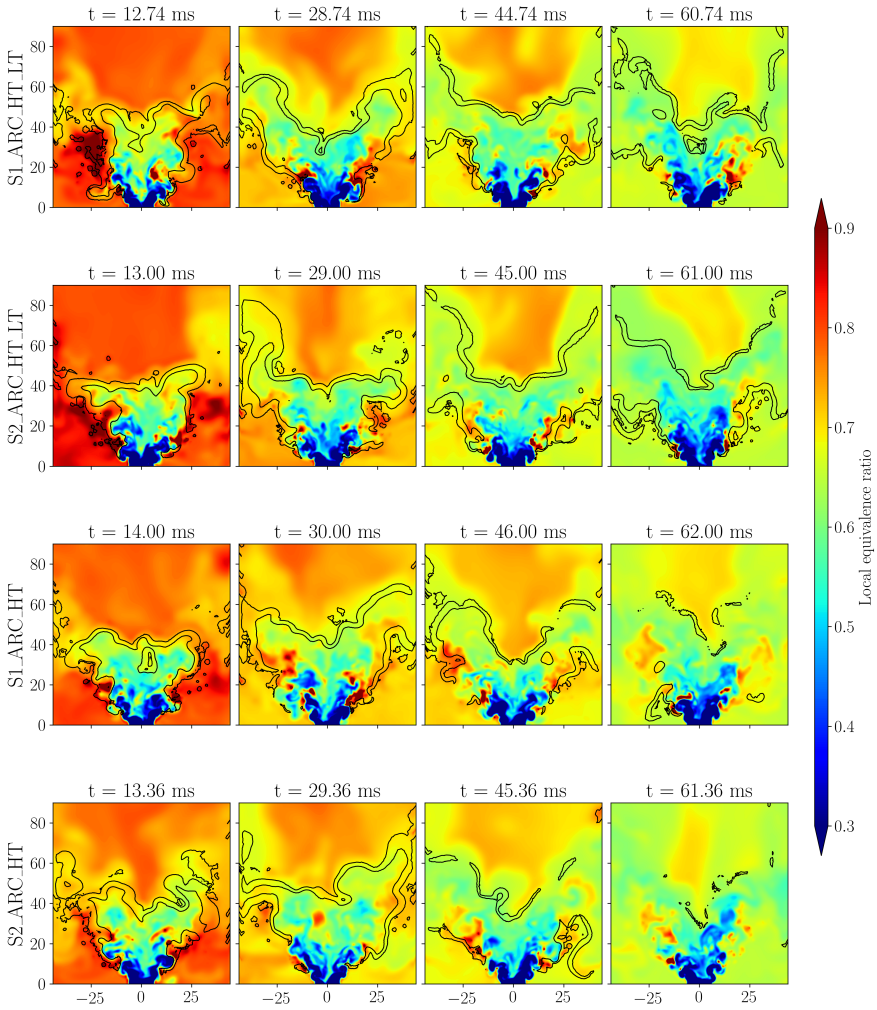

Figure 15: Time evolution of the local equivalence ratio in the central cut plane for the 4 cases studied. Black iso-line corresponds to a heat release rate of 5e7 W/m^3

Chemistry (ARC) mechanisms are used for that purpose.

Four cases are investigated in this study combining a variation of volatility due to a different composition and of the behavior at low temperature by the inclusion of the low-temperature chemistry pathways in one of the ARC mechanisms. One surrogate (S2) has a higher volatility than the other (S1). ARC_HT contains only high-temperature chemistry pathways whereas ARC_HT_LT contains both low- and high-temperature pathways. The 4 cases are labeled: S1_ARC_HT, S2_ARC_HT, S1_ARC_HT_LT and S2_ARC_HT_LT.

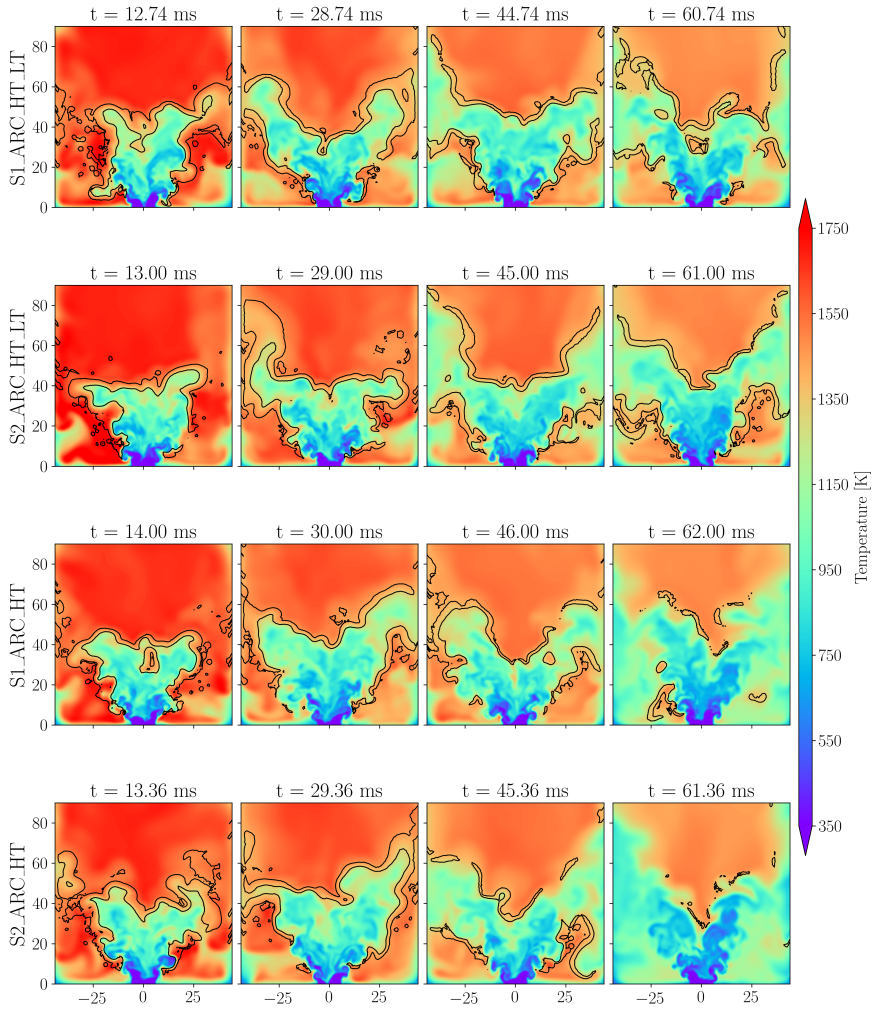

Figure 16: Time evolution of the temperature in the central cut plane for the 4 cases studied. Black iso-line corresponds to a heat release rate of 5e7 W/m^3

On a stable operating condition, the fours cases behave similarly showing the same M-shape flame. ARC_HT_LT cases exhibit slightly more intense flame branches near the ORZ while S2 cases shows a higher vaporization rate in the fresh gases leading to a higher gaseous fuel mass fraction at the flame foot. However, differences are marginal. Near LBO, the behavior is quite different as the ARC_HT cases see an extinction despite being at an experimentally stable operating conditions, while the flame in the ARC_HT_LT cases is stable. As the surrogates' volatility shows little influence on the results, the difference in behavior was attributed to the

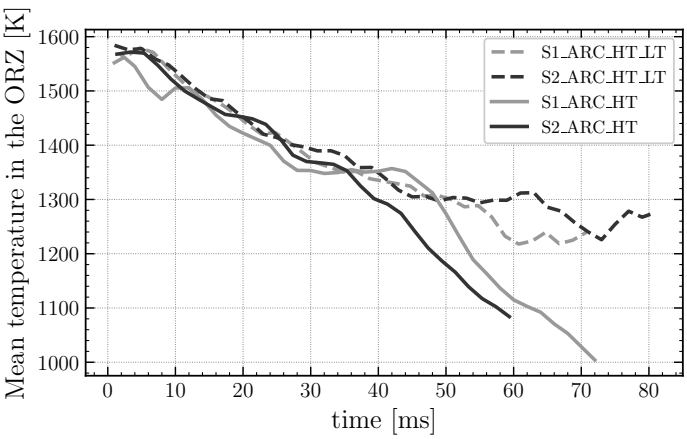

Figure 17: Evolution of the mean temperature in the ORZ from the stable point at ϕ=0.8 to the experimentally stable point near LBO (ϕ=0.6)

larger heat release rate in the flame branches near the ORZ that is sufficient to balance the heat losses in the ORZ and sustain a high temperature, which, in turn, helps stabilize the flame.

If this work focuses on the fuel model impact on the LBO prediction, other models that were not investigated here may impact the numerical results. Therefore, several other points should be addressed to provide a quantitative estimation of the LBO limit, such as the fuel injection and atomization models relying on a phenomenological approach in this work, or the sensitivity to the mesh resolution that may modify the flame response to turbulence and strain, especially when using the TFLES model. Nevertheless, even though this study provides qualitative results, a clear trend highlighting the importance of the inclusion of low-temperature chemistry pathways in reduced chemistry mechanisms to capture the fuel behavior near LBO is found.

ACKNOWLEDGEMENTS

This work was performed using HPC resources from GENCI-TGCC (Grant 2024-A0152B10157). We also acknowledge the EuroHPC Joint Undertaking for awarding this project access to the EuroHPC supercomputer LUMI, hosted by CSC (Finland) and the LUMI consortium through a EuroHPC Regular Access call.

REFERENCES

1. Hassan, H. and Pfaender, H. and Mavris, D.N. Feasibility analysis of aviation CO2 emission goals under uncertainty, *17th AIAA Aviation Technology, Integration, and Operations Conference*, 2017.
2. Undavalli, V. et al. Recent advancements in sustainable aviation fuels, *Progress in Aerospace Sciences*, 2023, **136**.

3. QASEM, N.A.A. ET AL. A recent review of aviation fuels and sustainable aviation fuels, *Journal of Thermal Analysis and Calorimetry*, 2024.
4. COLKET, M. ET AL. Overview of the national jet fuels combustion program, *AIAA Journal*, 2017, **55**, (4), pp. 1087-1104.
5. COLBORN, J.G. ET AL. Fuel and Operating Condition Effects on Lean Blowout in a Swirl-Stabilized SingleCup Combustor, *AIAA SciTech Forum*, Orlando 2020.
6. PEIFFER, E.E., HEYNE, J.S. and Colket, M. Characteristic Timescales for Lean Blowout of Alternative Jet Fuels in Four Combustor Rigs, *AIAA SciTech Forum*, Cincinnati 2020.
7. ROCK, N. ET AL. Liquid Fuel Property Effects on Lean Blowout in an Aircraft Relevant Combustor, *Journal of Engineering for Gas Turbines and Power*, 2019, **141**.
8. JONES, W.P. and TYLISZCZAK, A. Large Eddy Simulation of Spark Ignition in a Gas Turbine Combustor, *Flow Turbulence and Combustion*, 2010, **85**, pp. 711-734.
9. JONES, W.P., LYRA, S. and NAVARRO-MARTINEZ, S. Numerical investigation of swirling kerosene spray flames using Large Eddy Simulation, *Combustion and Flame*, 2012, **159**, pp. 1539-1561.
10. FRANZELLI, B. ET AL. A two-step chemical scheme for kerosene–air premixed flames, *Combustion and Flame*, 2010, **157**, pp. 1364-1373.
11. LIVEBARDON, T. ET AL. Combining LES of combustion chamber and an actuator disk theory to predict combustion noise in a helicopter engine, *Combustion and Flame*, 2016, **165**, pp. 272-287.
12. KUN, W. ET AL. A physics-based approach to modeling real-fuel combustion chemistry - IV. HyChem modeling of combustion kinetics of a bio-derived jet fuel and its blends with a conventional Jet A, *Combustion and Flame*, 2018, **198**, pp. 477-489.
13. RICHTER, S. ET AL. A combined experimental and modeling study of combustion properties of an isoparaffinic alcohol-to-jet fuel, *Combustion and Flame*, 2022, **240**, pp. 111994.
14. MEHL, M., PELUCCHI, M. and OSSWALD, P. Understanding the Compositional Effects of SAFs on Combustion Intermediates, *Frontiers in Energy Research*, 2022, **10**.
15. SHASTRY, V. ET AL. Numerical study of multicomponent spray flame propagation, *Proceedings of the Combustion Institute*, 2021, **38**, (2), pp. 3201-3211.
16. IBANEZ, J.P., NOCIVELLI, L. and DASGUPTA, D. Multi-component Evaporation of Sustainable Aviation Fuel Droplets, *AIAA SciTech Forum*, Orlando 2024.
17. RANZI, E. ET AL. Reduced kinetic schemes of complex reaction systems: Fossil and biomass-derived transportation fuels, *International Journal of Chemical Kinetics*, 2014, **46**, pp. 515-542.
18. FELDEN, A. ET AL. Including analytically reduced chemistry (ARC) in CFD applications, *Acta Astronautica*, 2019, **158**, pp. 444-459.
19. PIGNATELLI, F. ET AL. Predictions of Spray Combustion using Conventional Category A Fuels and Exploratory Category C Fuels, *AIAA SciTech Forum*, National Harbor 2023.
20. AKERBLOM, A. ET AL. Numerical Modeling of Chemical Kinetics, Spray Dynamics, and Turbulent Combustion towards Sustainable Aviation, *Aerospace*, 2024, **11**, (1).
21. SORIANO, B.S. ET AL. DNS of flame stabilization dynamics of a swirl-stabilized spray

burner using sustainable aviation fuels, *AIAA SciTech Forum*, Orlando 2024.

22. CORDIS - EU RESEARCH RESULTS JET Fuel SCREENing and Optimization, https://cordis.europa.eu/project/id/723525.
23. ECKEL, G. ET AL. LES of a swirl-stabilized kerosene spray flame with a multi-component vaporization model and detailed chemistry, *Combustion and Flame*, 2019, **207**, pp. 134-152.
24. WIRTZ, J. Modelling the impact of fuel aeronautical gas turbine, Phd Thesis, INPT, Toulouse, 2022.
25. SHASTRY, V. ET AL. Large Eddy Simulations of complex multicomponent swirling spray flames in a realistic gas turbine combustor, *Proceedings of the Combustion Institute*, 2023, **39**, (2), pp. 2693-2703.
26. KOOB, P. ET AL. Large Eddy Simulation of Soot Formation in a Real Aero-Engine Combustor Using Tabulated Chemistry and a Quadrature-Based Method of Moments, *Journal of Engineering for Gas Turbines and Power*, 2024, **146**.
27. IRIMIEA, C. ET AL. ALTERNATE: Experimental and modeling study of soot formation in high-pressure kerosene and SAF combustion, *Towards Sustainable Aviation Summit*, Toulouse 2022.
28. ESCLAPEZ, L. ET AL. Fuel effects on lean blow-out in a realistic gas turbine combustor, *Combustion and Flame*, 2017, **181**, pp. 82-99.
29. PANCHAL, A. and MENON, S. Large eddy simulation of fuel sensitivity in a realistic spray combustor II. Lean blowout analysis, *Combustion and Flame*, 2022, **240**, pp. 112161.
30. HASTI, V.R. ET AL. Computation of conventional and alternative jet fuel sensitivity to lean blowout, *Journal of the Energy Institute*, 2022, **101**, pp. 19-31.
31. LU, T. and LAW, C.K. Systematic approach to obtain analytic solutions of quasi steady state species in reduced mechanisms, *The Journal of Physical Chemistry*, 2006, **110**, (11), pp. 13202-13208.
32. ABRAMZON, B. and SIRIGNANO, W.A. Droplet vaporization model for spray combustion calculations, *International Journal of Heat and Mass Transfer*, 1989, **32**, pp. 1605-1618.
33. DOOLEY, S. ET AL. A jet fuel surrogate formulated by real fuel properties, *Combustion and Flame*, 2010, **157**, pp. 2333-2339.
34. KIM, D., MARTZ, J. and VIOLI, A. A surrogate for emulating the physical and chemical properties of conventional jet fuel, *Combustion and Flame*, 2014, **161**, pp. 1489-1498.
35. NARAYANASWAMY, K., PITSCH, H. and PEPIOT, P. A component library framework for deriving kinetic mechanisms for multi-component fuel surrogates: Application for jet fuel surrogates, *Combustion and Flame*, 2016, **165**, pp. 288-309.
36. WANG, H. ET AL. A physics-based approach to modeling real-fuel combustion chemistry - I. Evidence from experiments, and thermodynamic, chemical kinetic and statistical considerations, *Combustion and Flame*, 2018, **193**, pp. 502-519.
37. LUO, L. and LIU, Y.C. Variation of gas phase combustion properties of complex fuels during vaporization: Comparison for distillation and droplet scenarios, *Proceedings of the Combustion Institute*, 2021, **38**, pp. 3287-3294.
38. SILKE, E.J., CURRAN, H.J. and SIMMIE, J.M. The influence of fuel structure on combus-

tion as demonstrated by the isomers of heptane: a rapid compression machine study, *Proceedings of the Combustion Institute*, 2005, **30**, (2), pp. 2639-2647.

39. HALL, C. ET AL. Quantifiyng isomeric effects: A key factor in aviation fuel assessment and design, *Fuel*, 2024, **357**, pp. 129912.
40. CAZERES, Q. ET AL. A fully automatic procedure for the analytical reduction of chemical kinetics mechanisms for Computational Fluid Dynamics applications, *Fuel*, 2021, **303**.
41. PEPIOT-DESJARDINS, P. and PITSCH, H. An efficient error-propagation-based reduction method for large chemical kinetic mechanisms, *Combustion and Flame*, 2008, **154**, pp. 67-81.
42. PEPIOT-DESJARDINS, P. and PITSCH, H. An automatic chemical lumping method for the reduction of large chemical kinetic mechanisms, *Combustion Theory and Modelling*, 2008, **12**, pp. 1089-1108.
43. MOHADDES, D., XIE, W. and IHME, M. Analysis of low-temperature chemistry in a turbulent swirling spray flame near lean blow-out, *Proceedings of the Combustion Institute*, 2021, **38**, (2), pp. 3435-3443.
44. GROHMANN, J. ET AL. Influence of single-component fuels on gas-turbine model combustor lean blowout, *Journal of Propulsion and Power*, 2018, **34**, pp. 97-107.
45. CANTU, L. ET AL. Temperature measurements in confined swirling spray flames by vibrational coherent anti-stokes raman spectroscopy, *Experimental Thermal and Fluid Science*, 2018, **95**, pp. 52-59.
46. GROHMANN, J. ET AL. Investigation of differences in lean blowout of liquid single-component fuels in a gas turbine model combustor, *52nd AIAA/SAE/ASEE Joint Propulsion Conference*, Salt Lake City 2016.
47. AVBP SOLVER, *https://cerfacs.fr/avbp7x/*
48. LAX, P.D. and WENDROFF, B. Difference schemes for hyperbolic equations with high order of accuracy, *Communications on Pure and Applied Mathematics*, 1964, **17**, pp. 381-398.
49. CHARLETTE, F., MENEVEAU, C. and VEYNANTE, D. A power-law flame wrinkling model for LES of premixed turbulent combustion, part I: non-dynamic formulation and initial tests, *Combustion and Flame*, 2002, **131**, pp. 159-180.
50. JARAVEL, T. Prediction of pollutants in gas turbines using large eddy simulation, Phd Thesis, INPT, Toulouse, 2016.
51. YAMASHITA, H., SHIMADA, M. and TAKENO, T. A numerical study on flame stability at the transition point of jet diffusion flames, *Symposium (International) on Combustion*, 1996, **26**, pp. 27-34.
52. SANJOSÉ, M. ET AL. Fuel injection model for Euler-Euler and Euler-Lagrange Large-Eddy Simulations of an evaporating spray inside an aeronautical combustor, *International Journal of Multiphase Flow*, 2011, **37**, pp. 514-529.
53. POINSOT, T. and LELEF, S. Boundary Conditions for Direct Simulations of Compressible viscous flows, *Journal of Computational Physics*, 1992, **101**, pp. 104-129.
54. FICHET, V. ET AL. A reactor network model for predicting NOx emissions in gas turbines, *Fuel*, 2010, **89**, (9), pp. 2202-2210.

55. Lefebvre, A.H. and McDonell, V.G. Atomization and Sprays, 2nd Edition, 2017, CRC Press.

56. Pires, A.P.P., et al. Chemical Composition and Fuel Properties of Alternative Jet Fuels, *BioResources*, 2018, **13**, (2), pp. 2632-2657.

57. Buschhagen, T. et al. Effect of Aviation Fuel Type and Fuel Injection Conditions on Non-reacting Spray Characteristics of a Hybrid Airblast Fuel Injector, *AIAA SciTech Forum*, San Diego 2016.

APPENDIX

A. Cold flow validation

The accuracy of the LES is first assessed by comparing the numerical time-averaged velocity profiles to PIV measurements. Mean velocity profiles and RMS velocity profiles are presented in Fig. 18 and Fig. 19,respectively. The LES profiles (lines) match very closely the mean experimental velocity profiles. The main differences can be observed for the axial component of the velocity (y-axis) at a height of y = 30 mm. The central recirculation zone is predicted slightly larger compared to experiment. However, the overall agreement is really good. RMS velocity profiles show more discrepancies, especially towards the central axis of the burner where the levels predicted by the LES are significantly higher than the experimental results. There is also a difference in the results obtained at H=30mm. The LES matches closely one set of data (circle) whereas the other experimental set shows higher values (square). Even if differences exist between numerical and experimental results, the mean and RMS velocity profiles are globally well reproduced.

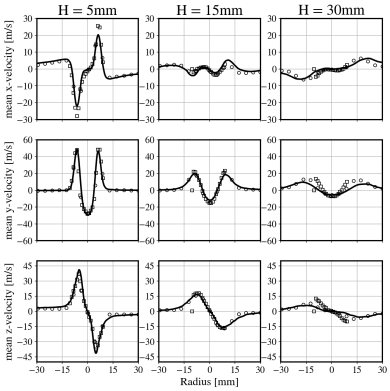

Figure 18: Time-averaged mean velocity profiles in the center plane for three heights in the burner: LES (lines) and 2 experimental sets of data (square and circle)

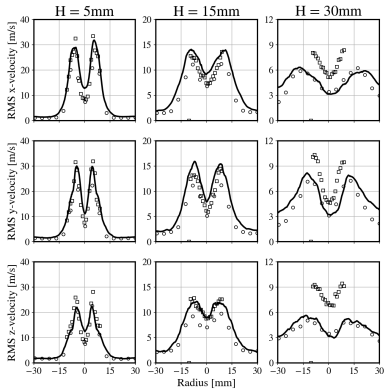

Figure 19: Time-averaged velocity fluctuations (RMS) profiles in the center plane for three heights in the burner: LES (lines) and 2 experimental sets of data (square and circle)

B. SMD sensitivity to operating conditions

The fuel physical properties were identified as key properties for the LBO phenomenom. A sensitivity analysis to the reduction of fuel mass flow rate and fuel property is carried out in this section. The prefilming airblast atomizer was characterized experimentally by[46]. Grohmann et al.[46] proposed the following parameters for a Lefebvre correlation[55]:

$$\frac{SMD}{l_c} = 0.1632\left(\frac{\sigma}{\rho_{air}U_{air}^2 d_i}\right)^{0.5}\left(1+\frac{\dot{m}_{fuel}}{\dot{m}_{air}}\right) + 0.022\left(\frac{\mu_{fuel}^2}{\sigma\rho_{fuel}d_i}\right)^{0.5}\left(1+\frac{\dot{m}_{fuel}}{\dot{m}_{air}}\right) \quad \ldots(1)$$

During the LBO procedure, the air mass flow rate is kept constant while the fuel mass flow rate is constant. Therefore, the evolution of the SMD throughout the LBO procedure can be estimated if the behavior of the prefilming airblast atomizer is not degraded (i. e. the pressure swirl spray still impacts the prefilming walls of the injection system). From the experimental correlation, the variation from $\phi = 0.8$ to $\phi_{\mathrm{LBO}} = 0.5$ would induce the following variation on the SMD:

$$\frac{SMD_{\phi=0.5}}{SMD_{\phi=0.8}} = 0.98 \quad \ldots(2)$$

From this analysis, it can be deduced that the variation of SMD during the LBO procedure is limited and taking into account its variation should have a limited impact on the LBO prediction. This holds as long as the behavior of the atomizer is not degraded.

As discussed in the manuscript, the numerical spray distribution was fitted for Jet A in a previous work[24]. When dealing with SAFs, one question arises: how is the spray distribution affected? This is also studied relying on the fitted Lefebvre correlation from[55]. Grohamnn et al.[46] have demonstrated that the correlation accurately describes the variation of SMD for simple species based on their physical properties. The correlation is then used to investigate the variation in SMD when changing the fuel.

The correlation highlights the importance of three liquid properties: surface tension, viscosity and density. Those three properties have been measured during the JETSCREEN campaign for JET-A, ATJ and HEFA (with the exception of surface tension for HEFA). They are reported in Table 5.

Table 6: Properties measured during the JETSCREEN campaign

	Jet A	**ATJ**	**HEFA**
σ [mN/m] at 20°C	25.35	22.88	
$\nu\left[\mathrm{mm^2/s}\right]$ at -20°C	3.379	5.322	4.126
$\rho\left[\mathrm{kg/m^3}\right]$ at 15°C	793.2	761.8	752

The surface tension of HEFA must be estimated to perform the sensitivity analysis. Pires et al.[56] reported an extensive study on aviation fuel properties in which 3 conventional fuels, 1 ATJ and 2 HEFA samples are studied. The surface tensions measured are reported in Table 6. The surface tension for then conventional fuels studied ranges between 24.6 and 26.7 mN/m whereas the ATJ has a surface tension of 22.2 mN/m. Those values show the same trend as the measurements from the JETSCREEN campaign even if the batches of fuel are different. Therefore, the value for surface tension of HEFA reported in Pires et al.[56] will be used to estimate the surface tension of the HEFA in JETSCREEN: a value of 23.8 mN/m is chosen.

Table 7: Surface tension reported in Pires et al.[56]

	Jet A s1	**Jet A s2**	**Jet A s3**	**ATJ**	**HEFA s1**	**HEFA s2**
σ [mN/m] at 20°C	25.8	26.7	24.6	22.2	23.5	24

To estimate the SMD variation with the fuel properties, some parameters in the correlation must be fixed. The air velocity is estimated from the maximum velocity observed in the non-reactive simulations: U_{air}=60m/s. The characteristic length is chosen to be equal to the prefilming diameter (8 mm). The air density is taken at the inlet condition: ρ_{air}=1.167kg/m^3. The mass flow rates are considered constant for each fuel and taken at the stabilized flame for Jet A at ϕ=0.8, reported in Table 4. Then, the SMD variation with the fuel can be estimated:

$$\frac{SMD_{ATJ}}{SMD_{JETA}} = 0.972 \qquad and \qquad \frac{SMD_{HEFA}}{SMD_{JETA}} = 0.977 \qquad \ldots(3)$$

Then, the SMD variations associated to a change of fuel are expected to be small. Therefore, the injected distribution is not modified in the simulation.

This sensitivity study is confirmed by a study of another combustor with a prefilming airblast injector. It is shown that the spray characteristics of these fuels have little correlation between fuel physical properties and droplet sizes[57]. This is likely because the combination of the airblast and air-assisted characteristic of the fuel nozzle result in droplet diameters that are relatively independent of the fuel properties. Hence, the spray characteristics are similar among fuels.